Chemical Engineering Science 65 (2010) 3025–3033

Contents lists available at ScienceDirect

Chemical Engineering Science

journal homepage: www.elsevier.com/locate/ces

Ab initio screening of metal sorbents for elemental mercury capture in syngas streams

Anubhav Jain [a], S.-A. Seyed-Reihani [b], Christopher C. Fischer [a], David J. Couling [b], Gerbrand Ceder [a], William H. Green [b,*]

[a] Department of Materials Science and Engineering, Massachusetts Institute of Technology, USA
[b] Department of Chemical Engineering, Massachusetts Institute of Technology, USA

ARTICLE INFO

Article history:
Received 16 September 2009
Received in revised form
17 January 2010
Accepted 22 January 2010
Available online 29 January 2010

Keywords:
Computational chemistry
Mercury
Coal gasification
Thermodynamics process
Gases
Energy

ABSTRACT

Coal gasification provides an opportunity to improve the thermal efficiency of energy extraction from coal over traditional pulverized coal technology, but efficiencies are hindered by low temperature removal of mercury and other pollutants. This work screens via density functional theory (DFT) calculations 22 pure metals as potential high-temperature Hg sorbents for coal gasification plants. The DFT enthalpy of amalgamation and oxidation is evaluated for each metal as indicators of their potential to either sorb Hg or oxidize in the gas stream. Our results predict Pd to be the most promising candidate for Hg removal, as it has the highest amalgamation enthalpy of all metals not expected to oxidize. No metals tested are ideal for Hg capture, as we find that amalgamation enthalpies correlate with oxidization enthalpies; thus, pure metals are either poor Hg adsorbers or strong oxidizers. Other chemical classes may be more promising as Hg sorbents; future work may apply the screening procedure discussed here to more complex compounds, such as binary and ternary alloys, oxides, and sulfides.

1. Introduction

Coal is a major energy source, currently supplying 25% of the world's energy needs and producing 40% of its electricity (Powell and Morreale, 2008). Forward-looking projections by the International Energy Agency indicate that under most scenarios, coal will continue to be a major energy source for many years to come (International Energy Agency, 2008). Unfortunately, coal power plants suffer from their pollution footprint; pollutants from coal power generation include the greenhouse gas CO_2, sulfur dioxide, and toxic metals such as cadmium, selenium, arsenic, and mercury. Responsible future use of coal as an energy source thus depends on discovering methods to reduce harmful emissions.

One promising technology to extract energy from coal is the integrated gasification combined cycle (IGCC). In this technique, coal is mixed with water vapor and oxygen and then gasified to produce a combustible *syngas*, a mixture of carbon monoxide and hydrogen gas. Power plants incorporating the IGCC are predicted to operate at a higher efficiency than traditional pulverized coal-fired plants (Nexant Inc., 2006) while also facilitating CO_2 capture, using less water, and generating less solid waste. Unfortunately, IGCC plants also suffer from pollution problems. The EPA has identified the neurotoxin mercury as a particularly harmful air pollutant and continues to work to reduce its emissions (Environmental Protection Agency Website, 2009, http://www.epa.gov/mercury/regs.htm). While the Clean Air Mercury Rule of 2005 (Environmental Protection Agency, 2005), which eventually mandated an approximately 70% reduction in mercury emissions from coal-fired plants, was recently vacated, many in the field expect even tighter Hg emissions standards in the future. As gasification technology use is expected to rise in use in the United States over the next 20 years (Granite et al., 2006), a low-cost mercury removal technique applicable to IGCC technology is urgently needed.

In general, mercury control options for IGCC applications focus on removing Hg prior to combustion, i.e. in the pre-combustion syngas mixture rather than the flue gas; as such, systems are cost-effective and maintain the efficiency of IGCC (Parsons Infrastructure & Technology Group Inc., 2002). Unfortunately, current sorbents reduce the overall efficiency of IGCC plants because they only operate well below combustion temperatures (approximately 260–315 °C) (Portzer et al., 2004), requiring the syngas stream to be cooled (in order to remove pollutants) and then subsequently re-heated. According to calculations by Eastman Chemical pertaining to the warm-temperature removal of H_2S (Schlather and Turk, 2007), increasing sorbent operating temperatures to the dew point of water in the syngas stream, approximately 170 °C (assuming 30 bar stream pressure and

* Corresponding author. Tel.: +1 617 253 4580.
E-mail address: whgreen@mit.edu (W.H. Green).

0009-2509/$ - see front matter © 2010 Elsevier Ltd. All rights reserved.
doi:10.1016/j.ces.2010.01.024

negligible HCl), (Electric Power Research Institute, 1998), would improve IGCC thermal efficiency up by 3.6%; i.e., electricity production would increase by almost 10%.

Efficient removal of mercury from the syngas stream without cooling is made challenging due to the low concentration of mercury in the stream and the high temperatures involved, both of which favor mercury's existence in the gas phase. In addition, reports indicate that between half and 97% of mercury emitted from IGCC plants is in elemental form (Pavlish et al., 2003; Portzer et al., 2004). This form is less reactive than the oxidized form, with removal even at lower temperatures often requiring surface oxidation (Lee et al., 2008).

Recently, several studies have investigated cost-competitive sorbents with high efficiency removal of elemental mercury from combustion flue gas products (Granite et al., 1998, 2000, 2006; O'Dowd et al., 2004; Poulston et al., 2007; Presto and Granite, 2008). Current sorbents for flue gas Hg removal that include activated carbon, metal oxides, metal sulfides, and metals only show high efficiency below ~150 °C (Granite et al., 1998, 2000); a satisfactory high-temperature Hg sorbent for IGCC applications has yet to be identified.

As several research groups now have experimental facilities for testing Hg sorbent performance on a small scale, what is needed in the field is a methodology by which to suggest new sorbent candidates. In this work, we use computational chemistry techniques to screen a large number of potential Hg sorbents applicable to the IGCC. The current investigation focuses on a well-studied chemical space – the pure metals – to validate our technique in reproducing experimental observations.

2. Methodology details

This work focuses on a particular type of sorbent in which elemental Hg in the gaseous state binds to a pure metal **M** to form a binary amalgam, i.e.

$$\mathbf{Hg}(g)+y\mathbf{M}\rightarrow\mathbf{HgM}_y \quad (1)$$

Although many metals, in particular the noble metals, are speculated to react with Hg in this manner in a gas stream (Granite et al., 2000), the purpose of our analysis is not to try to reproduce the mechanism by which Hg binds to sorbents. Instead, we compute the bulk formation enthalpies of reaction (1) for different metals as an *indicator* of Hg-metal bond strength.

The true performance of a sorbent depends on several complex factors, which include the mechanism by which Hg binds to the sorbent, sorbent particle size, mass transfer considerations, kinetics of capture, surface effects, residence time, and interaction with other gas constituents (Pavlish et al., 2003). However, we expect that despite these effects, amalgam formation enthalpy will strongly reflect the dominant effects associated with varying sorbent chemistry. In this work, we use *ab initio* computations to test the formation enthalpy for 70 different binary amalgam crystal structures from the Inorganic Crystal Structure Database (ICSD) (Bergerhoff et al., 1983; FIZ Karlsruhe, 2009), encompassing 65 distinct compositions of metal–mercury amalgams for 47 crystal structures of 22 metals in an effort to screen metals as Hg sorbents.

In addition to strong Hg binding, an additional design constraint is that the desired Hg sorbent must resist reacting unfavorably with other components of the syngas stream that are generally present in much higher concentrations than Hg. Based on Ellingham diagrams (Ellingham, 1944; Mitchell, 2004), we expect one of the most relevant issues for metals in a syngas stream to be the possibility of competing oxidation by steam via the reaction

$$\mathbf{M}+y\mathbf{H_2O}(g)\rightarrow\mathbf{MO}_y+y\mathbf{H_2}(g) \quad (2)$$

To account for this possibility, we evaluate for our potential sorbents the enthalpy of oxidation, i.e.

$$\mathbf{M}+y\mathbf{O_2}(g)\rightarrow\mathbf{MO_{2}}_y \quad (3)$$

which can yield enthalpies of reaction (2) by incorporating the experimental dissociation enthalpy of water vapor

$$y\mathbf{H_2O}(g)\rightarrow y\mathbf{H_2}(g)+1/2y\mathbf{O_2}(g) \quad (4)$$

While experimental metal oxidation enthalpies of the form of reaction (3) are largely tabulated, using computed *ab initio* oxidation enthalpies not only fills in missing data but also places our results within a unified computational framework. To evaluate the formation enthalpy of reaction (3), we calculate the total energies for 183 metal oxide crystal structures from the ICSD encompassing 72 binary oxide compositions. We then evaluate metals for their ability to capture mercury via reaction (1) while resisting oxidation via reaction (2), screening them as potential Hg sorbents fully *in silico*. It is important to emphasize that this technique can be generalized to more complex sorbents, e.g. metal oxides or metal sulfides, thus providing a systematic technique by which to suggest new candidate Hg sorbents.

2.1. Calculation details

Ab initio methods based on Density Functional Theory (DFT) are used to understand and predict a wide range of material properties. Such computational techniques are especially useful when experimental data is unavailable in the literature, such as when exploring novel materials or when obtaining experimental data proves particularly difficult (Hafner et al., 2006).

DFT requires as inputs structural data of a material as well as parameters relating to the choice of approximations and accuracy of the calculations. Our structural data was imported from the Inorganic Crystal Structure Database (ICSD) (Bergerhoff et al., 1983; FIZ Karlsruhe, 2009), which contains roughly 100,000 records of inorganic crystal structures. The energies of all of the compounds were evaluated using the Vienna Ab initio Simulation Package (VASP) (Kresse and Furthmuller, 1996). Projector augmented wave (PAW) potentials (Blochl, 1994; Kresse and Joubert, 1999), as distributed in the VASP package, were used throughout. Our calculations used the generalized gradient approximation (GGA) to DFT as formulated by Perdew et al., 1996. An automatic *k*-point mesh generation scheme distributed 500/(number of atoms in unit cell) *k*-points as uniformly as possible in *k*-space using a gamma-centered mesh for hexagonal cells and Monkhorst-packed grids for all other cells. *K*-point convergence was checked by running a subset of amalgams at a higher *k*-point density of 2500/(number of atoms in unit cell); the higher density calculations matched our initial formation enthalpies to ~1–2 kJ/mol-Hg (Table A1). Energy cutoffs were set at 1.3 times the maximum suggested energy cutoff of the constituents of a compound for the supplied PAW potentials (Kresse and Furthmuller, & January). Atomic positions and cell parameters were fully relaxed via a conjugate gradient algorithm in two separate relaxation runs with an energy tolerance of 5×10^{-5} eV for each run using the AFLOW algorithm (Curtarolo, 2003). A mixture of RMM and Davidson diagonalization was used. Where applicable, spin-polarized calculations were conducted using a ferromagnetic initial state. For the O_2 molecule, we

employed a fitted energy that corrected for overbinding within the GGA approximation as well as self-interaction errors when calculating formation enthalpies from metals, as described by Wang et al., 2006. DFT+U was employed for Ni and Mn oxides in a rotationally invariant form as described by Dudarev et al., 1998 using U=6.0 and U=3.9, respectively, as per Wang's method (Wang et al., 2006) using experimental data from Kubaschewski et al., 1993.

2.2. Enthalpy of formation and extension of results to stream conditions

If zero-point energy effects are regarded as small, the zero temperature, zero pressure enthalpy of formation ΔH of solid phases can be obtained directly from calculations by subtracting the DFT total energies of the reactant compounds from the products. Although this calculated formation enthalpy is not strictly accurate at finite temperatures or pressures, it is often a good approximation because solid phase heat capacity differences are small between similar solids, as are differences in coefficients of thermal expansion. Thus formation enthalpies under ambient conditions are often estimated using zero temperature, zero pressure calculated results.

2.2.1. Accuracy of ab initio calculations

The comparison between the experimental and calculated formation enthalpies for several metal-mercury amalgams is shown in Fig. 1. For experimental data collected near ambient conditions (designated by solid black circles), the agreement between the experiments and our calculations is good, with an average absolute error of roughly 8 kJ/mol. For a few of the transition metal amalgams, however, the calculated and experimental results do not agree nearly as well. In the case of MnHg (shown in gray) and NiHg (not shown), the calculated formation enthalpies show the compounds to be unstable, even though both compounds are known to exist (albeit with weak binding) (ASM International, 2009; de Boer et al., 1988). This indicates that either the quantum calculations or some of the experimental structure information are incorrect for these two compounds. Both Mn and Ni are unusual in their strong spin polarization that leads to ferromagnetic and antiferromagnetic phases in some Mn- and Ni-containing alloys, phosphides, and arsenides, and the spin state is very sensitive to the crystal structure (Fujii et al., 1991; Valkov and Golovchan, 2005). We speculate that this may be related to the failure of our DFT method, though calculations of MnHg and NiHg performed with a low-spin initialization gave similar results. It is also conceivable that electronic correlation or relativistic effects may be sources of error, as properly treating these effects has previously been reported important for Hg calculations (Gaston et al., 2006; Steckel, 2008). In the case of the Y and Zr amalgams, we do not know the source of the disagreement between the calculations and the experiments, but it is at least possible that there are inaccuracies in the experimental data. The data shown as white circles that include the Y and Zr amalgams, were collected at high temperatures, and there may have been difficulty correcting these high-temperature data to a low-temperature solid Hg reference state by (de Boer et al., 1988). It should be noted that published estimates (de Boer et al., 1988) for the enthalpy of formation of the Y–Hg amalgams also disagree with the reported experimental values, but agree with our DFT calculations to within 2, 4, and 24 kJ/mol-Hg for YHg_3, YHg_2, and YHg, respectively.

Although the accuracy of DFT in reproducing binary metal oxide formation enthalpies has been previously established (Wang et al., 2006), for completeness Fig. 2 compares our computed results with experimental values reported in the literature. The median error is about 4%, or 33 kJ/mol-O_2. Despite good accuracy overall, our results indicate that two classes of materials – peroxides and noble metal oxides – are not well reproduced within the PBE functional. As the peroxides show too negative formation enthalpies, the O_2^{2-} ion may be overbound. In addition, the reduced accuracy of the noble metal oxides may be an

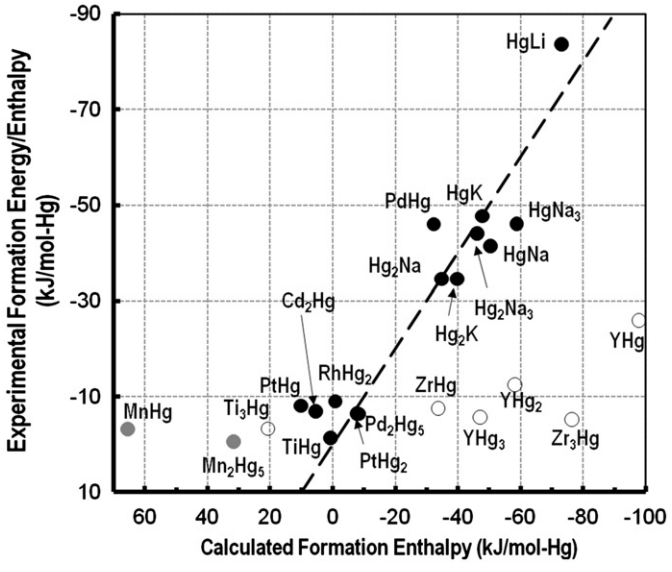

Fig. 1. Calculated DFT zero-pressure, zero-temperature formation enthalpies of metal–Hg amalgams versus solid phase enthalpies and energies listed in references (Hultgren et al., 1973) and (de Boer et al., 1988) (see Appendix Table A2 for further details). Open circles represent experimental data, which has been collected at high-temperature and subsequently extrapolated to room temperature in Ref. (de Boer et al., 1988); gray circles represent data we strongly suspect as failures of our computations.

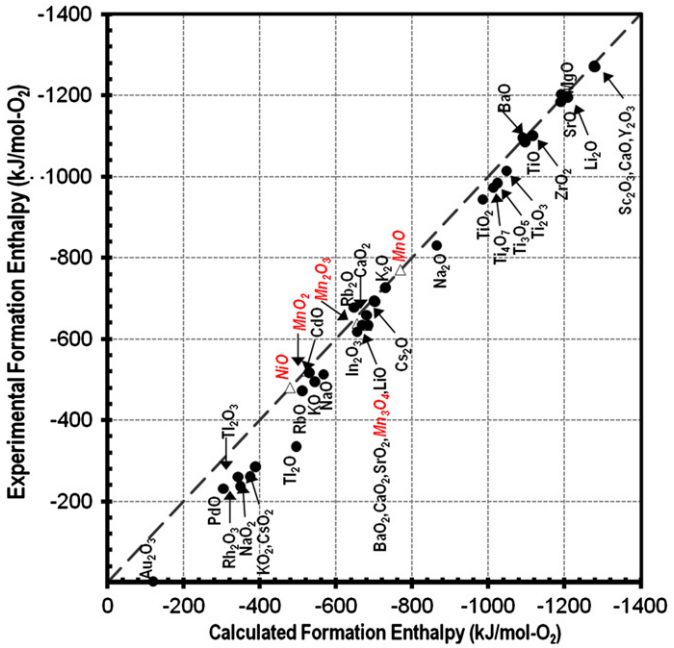

Fig. 2. Calculated DFT zero-pressure, zero-temperature formation enthalpies of binary metal oxides versus enthalpies reported in the literature (Binnewies, 1999; Dean, 1999; Kubaschewski et al., 1993; National Institute of Standards & Technology, 2009) (see Appendix Table A3 for further details). Ni and Mn compounds, for which a DFT+U correction was employed, are colored red, italicized, and are plotted as open triangles.

indication that DFT+U may be needed to describe correlated the *d* states in these materials, though this was not investigated further in this work (Wang et al., 2006).

2.2.2. Extension of calculated results to syngas stream environment

The primary aim of this work is to assess qualitative chemical trends in metal sorbents by examining bulk formation enthalpies. However, it is also possible to use our calculated data to determine whether a pure metal placed in a syngas environment will thermodynamically favor oxidization, amalgamation, or neither, through the use of a grand canonical thermodynamic potential. We model the syngas stream as an isothermal, isobaric system that is open to mercury, water vapor, and hydrogen gas, with the chemical potentials of these species controlled by temperature and their partial pressures in the gas stream. The water vapor and hydrogen gas equilibrium determines in our analysis the chemical potential of oxygen in the syngas stream. For open, isothermal, isobaric systems such as the modeled syngas, relative stability between different compounds is assessed by evaluating the grand canonical potential $\mathbf{\Phi}$, defined for the syngas as follows:

$$\mathbf{\Phi}(T,p,p_{H_2},p_{H_2O},p_{Hg}) = \mathbf{G}(T,p) - \boldsymbol{\mu}_{\mathbf{O_2}}(T,p_{H_2},p_{H_2O})\mathbf{x}_{\mathbf{O_2}} - \boldsymbol{\mu}_{\mathbf{Hg}}(T,p_{Hg})\mathbf{x}_{\mathbf{Hg}} \quad (5)$$

In Eq. (5), $\mathbf{G}$ represents the Gibbs free energy of the solid, $\boldsymbol{\mu}_{\mathbf{i}}$ represents the chemical potential of species *i*, and $\mathbf{x}_{\mathbf{i}}$ represents the fraction of species *i* in the compound (normalized per metal atom). The temperature T is the desired sorbent operating temperature, p is the total pressure of the syngas stream, and p_i represents the partial pressure of species *i*. For each sorbent candidate, we evaluate $\mathbf{\Phi}$ for the amalgam, oxide, and metal phases to predict the thermodynamically stable compound in the syngas stream. Sorbents that show a lower value of $\mathbf{\Phi}$ for the amalgam than the oxide and the pure metal are likely to be promising candidates for further investigation.

In order to evaluate $\mathbf{\Phi}$ using only our ground state DFT calculations and available thermodynamic data, a few simplifying assumptions need to be made. The most important assumption is that we neglect finite temperature effects for condensed phases when evaluating $\mathbf{G}$, $\boldsymbol{\mu}_{\mathbf{O_2}}$, and $\boldsymbol{\mu}_{\mathbf{Hg}}$. This assumption is appropriate because finite temperature effects arising from condensed phases are generally quite small when compared to effects arising from gas phase entropies. Thus, a good approximation for $\mathbf{\Phi}$ can be found by considering temperature for gas phases only. Other assumptions are that gas phase species can be treated under the ideal gas law, and that metal phases do not undergo phase transitions between 0 K and the sorbent operating temperature.

These simplifying assumptions allow us to approximate the components of $\mathbf{\Phi}$

$$\mathbf{G_{solids}}(T,p) \sim \mathbf{E}_{calc}(0\,K, 0\,atm) \quad (6)$$

$$\boldsymbol{\mu}_{\mathbf{Hg}}(T,p_{H_2},p_{H_2O}) \sim \mathbf{h}_{Hg}(T,p_0) + \Delta\mathbf{h_{vap}}(T) - \mathbf{T}[\mathbf{s}_{\mathbf{Hg}}(T,p_0) + \Delta\mathbf{s_{vap}}(T) - \mathbf{k}\ln(\mathbf{p_{Hg}}/\mathbf{p_0})] \quad (7)$$

$$\boldsymbol{\mu}_{\mathbf{O_2}}(T,p_{H_2},p_{H_2O}) \sim \mathbf{h}_{\mathbf{O_2}}(T,p_0) - T[\mathbf{s}_{\mathbf{O_2}}(T,p_0) - \mathbf{k}\ln(\mathbf{p}_{\mathbf{O_2}}(p_{H_2O},p_{H_2})/\mathbf{p_0})] \quad (8)$$

In these expressions, $\mathbf{h}$ represents enthalpy and $\mathbf{s}$ represents entropy, and both are evaluated at T and p_0 minus their solid phase temperature contributions (though includes their 0 K energy). The vaporization enthalpies and entropies of Hg, $\Delta\mathbf{h_{vap}}$ and $\Delta\mathbf{s_{vap}}$, are added to account for mercury's phase transition from a condensed (liquid) phase at standard pressure p_0 to a gas at the syngas pressure.

Because we are subtracting out solid phase temperature effects, the enthalpies $\mathbf{h_{Hg}}$ and $\mathbf{h_{O_2}}$ are equivalent to the calculated DFT total energy of bulk Hg solid and the fitted O_2 molecule energy (as described in Section 2.1), respectively, plus a PV term. We set the PV term to kT by the ideal gas law. In addition, $\mathbf{s_{Hg}}(T,p_0)$ is approximated as zero since Hg remains condensed (liquid) at standard pressure for syngas temperatures of interest. Again, the expectation is that this term will largely cancel with solid phase entropies, which are excluded from $\mathbf{G}$ in Eq. (6). The vaporization pressure of Hg was determined by experimental fits to the Antoine equation (Table 1). The vaporization enthalpy $\Delta\mathbf{h_{vap}}$ of Hg at the vaporization pressure and syngas temperature was approximated from the experimental data (Table 1). The vaporization entropy $\Delta\mathbf{s_{vap}}$ is taken as $\Delta\mathbf{h_{vap}}/T$, where T represents the syngas temperature. Finally the entropy of oxygen gas $\mathbf{s}_{\mathbf{O_2}}(T,p_0)$ was determined via experimental fittings to the Schomate equation (Table 1).

Because the syngas stream operates in a reducing environment, we do not expect metal oxidation to occur directly by O_2 gas. However, we do consider oxidation through steam; by setting oxygen in equilibrium with hydrogen gas and water vapor in the stream, we evaluate the effective partial pressure of oxygen $\mathbf{p}_{\mathbf{O_2}}(T,p_{H_2O},p_{H_2})$

$$\ln \mathbf{p}_{\mathbf{O_2}}(T,p_{H_2},p_{H_2O}) \sim 2[\Delta G^{\mathbf{rxn}}_{\mathbf{H_2O}}(T)/\mathbf{RT} - \ln \mathbf{p}_{\mathbf{H_2O}} + \ln \mathbf{p}_{\mathbf{H_2}}] \quad (9)$$

Here, $\Delta G^{\mathbf{r\times n}}_{\mathbf{H_2O}}$ is the Gibbs free energy associated with splitting water vapor into oxygen and hydrogen gas, modeled as a function of temperature from experimental parameters (Table 1).

Table 1
Experimental parameters used to evaluate $\mathbf{\Phi}$.

Parameter	Value
Δh_{vap} for Hg	59.1 kJ/mol (Fermi, 1956; Velasco et al., 2006)
Antoine equation for p_{vap}	$\log_{10}(p_{vap}) = A - B/(T+C)$ (bar)
Antoine parameters for Hg	A=4.858, B=3007.129, C=−10.001 (National Institute of Standards Technology, 2009)
Equation for gas entropies	$A\ln(T') + BT' + 1/2CT'^2 + 1/3DT'^3 - 1/2E/(T')^2 + G$ (J/mol*K) (National Institute of Standards Technology, 2009)
Equation for gas enthalpies	$AT' + 1/2BT'^2 + 1/3CT'^3 + 1/4DT'^4 - E/(T') + F - H$ (J/mol*K) (National Institute of Standards Technology, 2009)
O_2 gas parameters for h_{O_2} & s_{O_2}	A=31.322, B=−20.235, C=57.866, D=−36.506, E=−0.00737, F=−8.903, G=246.795, H=0.0, $T'=T/1000$ (National Institute of Standards Technology, 2009)
H_2 gas parameters for h_{H_2} & s_{H_2}	A=33.066, B=−11.363, C=11.433, D=−2.773, E=−0.159, F=−9.981, G=172.708, H=0.0, $T'=T/1000$ (National Institute of Standards Technology, 2009)
H_2O gas parameters for h_{H_2O} & s_{H_2O}	A=30.092, B=6.833, C=6.793, D=−2.534, E=0.0821, F=−250.881, G=223.397, H=−241.826, $T'=T/1000$ (National Institute of Standards Technology, 2009)
Equation for $\Delta G^{\mathbf{r\times n}}_{\mathbf{H_2O}}$	$h_{O_2} + h_{H_2}h_{H_2O} - T(s_{O_2} + sH_2 - sH_2O)$

Having derived approximations for many of the components of Φ, the remaining quantities needed are the partial pressures of the relevant species in the gas stream: $\mathbf{p_{Hg}}$, $\mathbf{p_{H_2O}}$, and $\mathbf{p_{H_2}}$. A typical syngas stream profile is shown in Table 2; using this as a reference, we set the partial pressure of Hg, $\mathbf{p_{Hg}}$, for our model stream as 10 ppb by volume ($\sim$100 ppbw) of the total syngas pressure of 30 bar, or 3×10^{-7} bar. We also choose for our model stream equal pressures of H_2O and H_2 (30% each), which is somewhat oxidizing.

3. Calculation results

The results of our DFT formation enthalpy calculations are presented in Tables A2 and A3 in the Appendix. For each composition, only the formation enthalpy of the most stable crystal structure amongst those found in ICSD (as determined by our calculations) is presented for conciseness and clarity. When looking solely at amalgam formation enthalpy trends (Table A2), the alkali earth metals and Li stand out as the most promising candidates for mercury removal since they bind Hg strongly (up to about -100 kJ/mol-Hg). However, it is important to remember that a candidate sorbent must also resist reactions with other gas constituents that could potentially render the sorbent ineffective for Hg removal. In particular, the alkali and alkali earth metals, while showing strong amalgam formation enthalpies, also have large oxidation enthalpies indicating that they will likely oxidize in the syngas stream (Table A3). More generally, the data shows that amalgam formation and oxidation are not independent variables that can be freely varied in the space of possible chemistries; rather, metals that form strong amalgams are also strong oxide-formers.

We can explain this trend roughly through simple chemical arguments. The alkali and alkali earth metals may form strong Hg amalgams by donating a large portion of their electron density to the more electronegative Hg. However, because oxygen is much more electronegative than Hg, oxidation enthalpies for these metals will be much larger than amalgamation enthalpies, making them difficult to use as sorbents. On the opposite end, metals that resist oxidation, such as the transition metals and noble metals, are near Hg on the periodic table. Thus there will not be a tendency for them to form strong polar bonds, and they may be stabilized by weak metallic alloying effects.

To understand the compromise between amalgamation and oxidation more clearly, we plot for each metal the mercury amalgam formation enthalpy per mol-Hg versus the binary oxide formation enthalpy per mol-O_2 (Fig. 3). When normalized in this manner, the formation enthalpies indicate the minimum chemical potential of Hg or O_2 gas needed before the metal favors forming the amalgam or oxide, respectively. In the case where multiple amalgams or oxides are present for a metal, we choose the composition having the lowest chemical potential for Hg or O_2, respectively. We also show as dashed lines in Fig. 3 the chemical potentials of oxygen gas and mercury in a syngas stream, as determined by the methods in Section 2.2.2. The chemical potentials are presented for the target temperature of 170 °C, the dew point of water vapor in the syngas stream. These chemical potential lines can be used to quickly predict whether a pure metal will amalgamate or oxidize when placed in the syngas stream. If the minimum chemical potential of Hg or O_2 in the metal compound is less than that of the respective gas species in the stream, the metal is thermodynamically predicted to react with that species in the syngas stream. Thus, metals in Fig. 3 above the chemical potential line of oxygen gas are estimated to form oxides in the syngas stream. Metals to the right of the chemical potential line of Hg gas are estimated to form amalgams

Table 2
Typical constituents and volume fractions of a syngas stream (Environmental Protection Agency, 2006).

Compound	Concentration (vol%)
CO	30–60
H_2	25–30
CO_2	5–15
H_2O	2–30
CH_4	0–5
H_2S	0.2–1
COS	0–0.1
N_2	0.5–4
Ar	0.2–1
NH_3+HCN	0–0.3
Hg	10 ppb

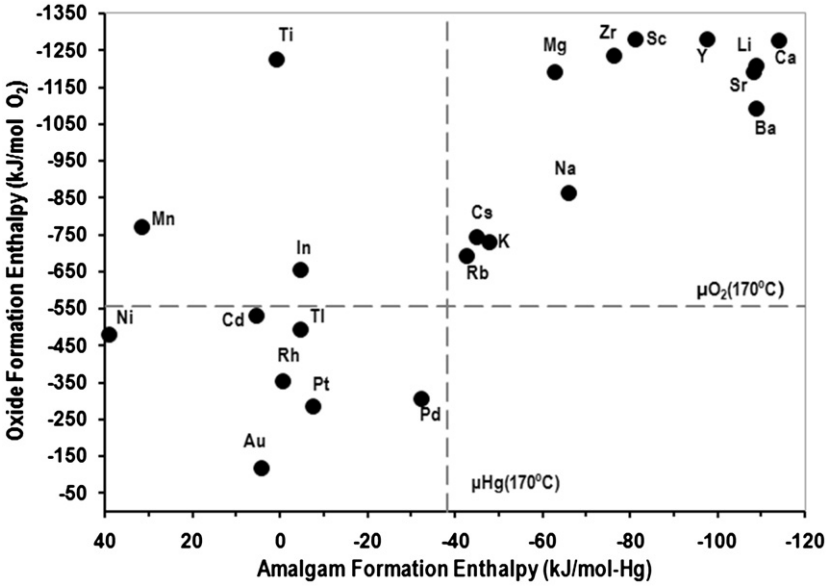

Fig. 3. Calculated amalgam formation enthalpies of binary Hg amalgam versus binary oxide, normalized per mol of Hg and per mol of O_2, respectively, to give estimates of mercury and oxygen chemical potentials. Dashed lines indicate our modeled chemical potential of oxygen and mercury in the syngas stream, as described in Section 2.2.2.

in the stream. Metals satisfying both criteria, in the upper right of the chart, must be evaluated via the grand canonical potential (Section 2.2.2) to find the most stable compound. This analysis predicts that all of these compounds will form oxides rather than amalgams. The most desirable metals would fall in the bottom-right region of the chart, where they would be predicted to amalgamate without oxidizing.

The only metal predicted by our calculations to be close to the energy range of amalgamation at 170 °C and 10 ppb Hg is Pd. To bring the Hg chemical potential line to the Pd amalgam formation enthalpy, one would need to increase the Hg concentration to approximately 50 ppb, or alternatively cool the stream to 143 °C. However, we emphasize that there are a number of important factors neglected when using bulk properties to model surface phenomena, so these numbers should be regarded as estimates rather than accurate predictions. Recently, some evidence of amalgamation has been found by Granite et al. when characterizing the surface of Pd/Al_2O_3 sorbents at 240 ppb Hg in a simulated syngas and between 204 and 371 °C (Baltrus et al., 2008), though more comprehensive characterization work remains in this area.

Other promising candidates are also noble metals as they show the highest amalgam formation enthalpies without oxidizing. Indeed the noble metals have been studied experimentally for some time and are widely considered the most promising metal Hg sorbents (Granite et al., 1998, 2006; Granite et al., 2000; Poulston et al., 2007). Our work not only confirms this trend, but singles out Pd as the most promising noble metal since its amalgam formation enthalpy is significantly higher than that of Pt, Rh, and Au. Pd is now regarded as a standout amongst the noble metals as a Hg sorbent (Granite et al., 2006). The metal Ti was experimentally found to sorb Hg in a nitrogen environment but not in a simulated syngas environment (Granite et al., 2006); such a result could be inferred from our plot, in which Ti is shown to have moderate Hg formation enthalpies but is predicted to be quite prone to oxidation in syngas environments.

The alkali metals Na, K, Cs, and Rb show lower oxidation enthalpies than the alkali earth metals, and higher amalgam formation enthalpies than the noble metals. This makes them appear like a fair compromise between optimizing amalgamation and oxidation behavior. However, the oxidation enthalpy of these metals may still be too high to avoid oxidation; of greater concern may be the tendency of alkali metals to react with steam to form hydroxides, which was not evaluated in this work.

Finally, we note that a previous study by Granite has examined the metals Ag, Ru, Ir as possible Hg sorbents in syngas environments (Granite et al., 2006). The metal Ag was not found to sorb mercury well (Granite et al., 2006). Both Ru and Ir showed Hg removal comparable to Pt in a nitrogen environment, but negligible Hg capacity in a syngas environment (Granite et al., 2006). None of these metals is present in our work due to a lack of structural data of Hg amalgams in the ICSD. Calculation of oxidation enthalpies of RuO_2 and IrO_2 yielded -421.6 and -361.4 kJ/mol-O_2, respectively, which are closer to the oxidation line than Pt (but still below the line). The failure of Ru and Ir in syngas streams may be because oxidation is more favorable for these metals than for Pt.

We note that our bulk calculations produce similar qualitative results to two studies of Hg adsorption on metal surfaces – a DFT study performed by Steckel, 2008 and the thermochromatography measurements by Soverna et al., 2005. The DFT study by Steckel predicts increasing Hg-metal reactivity in the order $Ag < Au < Cu < Ni < Pt < Pd$ (Steckel, 2008). This is consistent with our work, with two exceptions. We do not report data for Ag or Cu because structural data of Hg amalgam phases for these metals is lacking in the ICSD. In addition, this study found Ni to be less reactive with Hg than Au, which is in disagreement with the surface adsorption order reported by Steckel. Though this may represent a true difference between bulk and surface properties, it could also be caused by structural issues or a failure of PBE within our Ni calculations as described in Section 2.2.1. The sequence of Hg-metal reactivity as measured by thermochromatography studies of Sovera et al. increased as $Ag < Ni < Au < Pd < Pt$ (Soverna et al., 2005). The current work is in agreement with this order, with the exception that this work found Pd to interact more strongly with Hg than Pt. It is unclear whether this latter disagreement is due to inaccurate experimental numbers caused by difficulty in obtaining samples of Pt and Pd free of oxidation, as stated by Soverna et al., 2005 in their work, or due to a failure in the DFT method. The more detailed DFT surface calculations by Steckel, 2008 are in agreement with our work (i.e., Pd is found to bind Hg more strongly than Pt). However, the experimental adsorption capabilities of Hg in a simulated syngas as measured by Granite show Pt to have better low-temperature Hg adsorption capabilities and Pd to have better high-temperature Hg adsorption capabilities (Granite et al., 2006). Thus, it is still unclear whether Pt or Pd surfaces sorb Hg more strongly.

In conclusion, DFT tests of 22 metals did not yield a satisfactory new candidate for use as a Hg sorbent. However, they reproduced previously measured reactivity trends of surface phenomena and correctly identified the noble metals as promising Hg sorbent candidates. Further computations could be aimed at retaining the resistance to oxidation of the noble metals while improving Hg amalgamation strength towards the level of the alkali earth compounds, e.g. by alloying. Alternatively, completely different chemical classes, e.g. sulfides or oxides, which have thus far only received marginal attention (Granite et al., 1998) may be tested via DFT methods. While not pursued in this work, techniques are now available for the prediction of unknown crystal structures (Fischer et al., 2006). Thus, our methodology can be extended well beyond the space of structures present in experimental databases such as the ICSD, thereby allowing many new chemical combinations to be tested via quantum chemistry.

4. Conclusion

The discovery of high-temperature Hg sorbents for syngas applications is a complex optimization challenge, which has thus far been guided almost exclusively by a relatively small number of experimental studies. We believe that *ab initio* computational screening can quickly guide experiments towards promising sorbent materials. This paper demonstrates that relatively simple bulk calculations using structural data from online databases can predict qualitative experimental trends that highlight specific materials. Specifically, this study found noble metal sorbents to be interesting Hg sorbents, with no new interesting pure metal candidates for Hg sorbents with better performance than Pd. It should be straightforward to extend our technique to screen wider, more unexplored regions of chemical space prior to proceeding with experiments. Such a strategy would focus experiments towards materials proven to be viable computationally, greatly accelerating the pace at which new mercury sorbents are found.

Acknowledgements/Funding

This research was supported by the US Department of Energy through Grants no. #DE-FG02-96ER4557 and DE-FG02-97ER25308. The Green group would like to acknowledge funding from BP. The authors would like to thank Dr. Denis Kramer and Dr. Rickard Armiento for their helpful discussions, as well as Geoffroy Hautier and Charles Moore for their assistance with calculations.

Appendix A

See Tables A1–A3.

Table A1
Calculated zero-temperature, zero pressure binary amalgam formation enthalpies using two different numbers of *k*-points for all components in the reaction. The calculations using a *k*-point mesh with 500 *k*-points/atom per unit cell match those with 2500 *k*-points/atom per unit cell to within 1–2 kJ/mol-Hg.

Formula sum amalgam	Spacegroup amalgam (Bergerhoff et al., 1983; FIZ Karlsruhe, 2009)	Calc. formation enthalpy (kJ/mol-Hg) *k*-points*atoms=500	Calc. formation enthalpy (kJ/mol-Hg) *k*-points*atoms=2500
Li_3Hg	F m −3 m	−108.8	−110.4
LiHg	P m −3 m	−73.2	−73.0
MnHg	P 4/m m m	65.5	65.6
Mn_2Hg_5	P 4/m b m	31.6	31.6
Na_3Hg	R −3 m H	−58.8	−59.3
Na_8Hg_3	R −3 c H	−66.0	−64.7
Na_3Hg_2	P 42/m n m	−46.0	−45.0
NaHg	C m c m	−50.3	−51.2
$NaHg_2$	P 6/m m m	−34.7	−35.7
PdHg	P 4/m m m	−32.3	−32.7
Pd_2Hg_5	P 4/m b m	−8.3	−8.2
PtHg	P 4/m m m	10.3	9.7
$PtHg_2$	P 4/m m m	−7.7	−8.5
YHg	P m -3 m	−97.8	−100.0
YHg_2	P 6/m m m	−58.2	−59.1
YHg_3	P 63/m m c	−47.0	−47.1

Table A2
Calculated zero-temperature, zero pressure binary amalgam formation enthalpies from VASP along with ICSD space group. Known experimental formation enthalpies with a solid-state Hg reference are also indicated. Experimental numbers with an asterisk (*) indicate data collected at high or unknown temperatures, and later extrapolated to a solid Hg reference state by reference (de Boer et al., 1988).

Formula sum amalgam	Spacegroup amalgam (Bergerhoff et al., 1983; FIZ Karlsruhe, 2009)	Calc. formation enthalpy (kJ/mol-Hg)	Exp. formation enthalpy (kJ/mol-Hg)
Au_6Hg_5	P 63/m c m	4.2	
Ba_2Hg	I 4/m m m	−108.8	
BaHg	P m −3 m	−99.6	
$BaHg_2$	I m m a	−70.8	
$BaHg_{11}$	P m −3 m	−18.6	
Ca_5Hg_3	I 4/m c m	−112.8	
Ca_3Hg_2	P 4/m b m	−114.1	
CaHg	P m −3 m	−107.9	
$CaHg_2$	P 6/m m m	−64.3	
Ca_4Hg_9	P −4 3 m	−55.1	
$CaHg_{11}$	P m −3 m	−8.3	
Cd_2Hg	I 4/m m m	5.4	−6.9 (Hultgren et al., 1973)
$CdHg_2$	I 4/m m m	5.8	
CsHg	P −1	−45.2	
$CsHg_2$	I m m a	−38.1	
Cs_5Hg_{19}	I 4/m	−27.5	
Cs_3Hg_{20}	P m −3 n	−19.3	
InHg	R −3 m H	−4.6	
KHg	P −1	−47.8	−47.7 (Hultgren et al., 1973)
K_5Hg_7	P b c m	−43.8	
KHg_2	I m m a	−39.8	−34.5 (Hultgren et al., 1973)
K_2Hg_7	P −3 m 1	−26	
K_3Hg_{11}	I m m m	−25.1	
KHg_{11}	P m −3 m	−11.6	
Li_3Hg	F m −3 m	−108.8	
LiHg	P m −3 m	−73.2	−83.7 (Hultgren et al., 1973)
Mg_3Hg	R 3 2 H	−47	
Mg_2Hg	P n m a	−62.9	
Mg_5Hg_3	P 63/m c m	−54.2	
MgHg	P m −3 m	−42.1	
$MgHg_2$	I 4/m m m	−16.7	
MnHg	P 4/m m m	65.5	−3.2 (de Boer et al., 1988)*
Mn_2Hg_5	P 4/m b m	31.6	−0.6 (de Boer et al., 1988)*
Na_3Hg	R −3 m H	−58.8	−46.0 (Hultgren et al., 1973)
Na_8Hg_3	R −3 c H	−66	
Na_3Hg_2	P 42/m n m	−46	−44.0 (Hultgren et al., 1973)
NaHg	C m c m	−50.3	−41.4 (Hultgren et al., 1973)
$NaHg_2$	P 6/m m m	−34.7	−34.5 (Hultgren et al., 1973)
NiHg	P 4/m m m	38.9	
PdHg	P 4/m m m	−32.3	−46.0 (de Boer et al., 1988)
Pd_2Hg_5	P 4/m b m	−8.3	−6.4 (de Boer et al., 1988)
PtHg	P 4/m m m	10.3	−8.1 (de Boer et al., 1988)
$PtHg_2$	P 4/m m m	−7.7	−6.5 (de Boer et al., 1988)
$Rb_{15}Hg_{16}$	I 41/a Z	−42.7	
$RbHg_2$	I m m a	−38.4	
Rb_2Hg_7	P −3 m 1	−26.6	
Rb_5Hg_{19}	I 4/m	−26.3	
Rb_3Hg_{20}	P m −3 n	−17.3	
$RbHg_{11}$	P m −3 m	−12.5	
$RhHg_2$	P 4/m m m	−0.8	−9.0 (de Boer et al., 1988)
ScHg	P m −3 m	−81.4	
$ScHg_3$	P 63/m m c	−29.7	
Sr_3Hg_2	P 4/m b m	−108.5	
SrHg	P m −3 m	−102.9	
$SrHg_2$	P 6/m m m	−70.1	
Ti_3Hg	P m −3 m	20.7	−3.3 (de Boer et al., 1988)*
TiHg	P 4/m m m	0.7	−1.4 (de Boer et al., 1988)
TlHg	P m −3 m	−4.8	
$TlHg_3$	P m −3 m	−4.6	
YHg	P m −3 m	−97.8	−26.0 (de Boer et al., 1988)*
YHg_2	P 6/m m m	−58.2	−12.5 (de Boer et al., 1988)*
YHg_3	P 63/m m c	−47	−5.7 (de Boer et al., 1988)*
Zr_3Hg	P m −3 n	−76.4	
ZrHg	P 4/m m m	−33.7	−7.6 (de Boer et al., 1988)*
$ZrHg_3$	P m −3 m	−8.6	−5.2 (de Boer et al., 1988)*

Table A3
Calculated zero-temperature, zero pressure binary oxide formation enthalpies from VASP along with ICSD spacegroup. Known experimental formation enthalpies are also indicated.

Formula sum oxide	Spacegroup oxide	Calc. formation enthalpy (kJ/mol-O_2)	Exp. formation enthalpy (kJ/mol-O_2)
Au_2O_3	F d d 2	−119.4	−2.3 (Kubaschewski et al., 1993)
BaO	F m −3 m	−1090.3	−1096.2 (Kubaschewski et al., 1993)
BaO_2	I 4/m m m	−669.5	−634.3 (Kubaschewski et al., 1993)
CaO	F m −3 m	−1278	−1269.8 (Kubaschewski et al., 1993)
CaO_2	F 4/m m m	−680.5	−659 (Binnewies, 1999)
CdO	F m −3 m	−530	−516.8 (Kubaschewski et al., 1993)
CdO_2	P a −3	−290	
$Cs_{11}O_3$	P 1 21/c 1	−742.1	
Cs_3O	P 63/m c m	−740.6	
Cs_2O	R −3m H	−701.6	−692 (Kubaschewski et al., 1993)
CsO	I m m m	−524.1	
CsO_2	I 4/m m m	−388.6	−286.2 (Kubaschewski et al., 1993)
CsO_3	P 1 21/c 1	−301	
In_2O_3	I a −3	−655.2	−617.3 (Kubaschewski et al., 1993)
K_2O	F m −3 m	−730	−726.4 (Kubaschewski et al., 1993)
KO	C m c a	−544.8	−495 (Kubaschewski et al., 1993)
KO_2	F 4/m m m	−388.3	−284.5 (Kubaschewski et al., 1993)
KO_3	I 4/m c m	−301.1	
Li_2O	F m −3 m	−1208.2	−1195.8 (Kubaschewski et al., 1993)
LiO	P 63/m m c	−684.8	−633.9 (Kubaschewski et al., 1993)
MgO	F m −3 m	−1191.2	−1203.2 (Kubaschewski et al., 1993)
MgO_2	P a −3	−632.1	
MnO	F m −3 m	−769.4	−769.8 (Kubaschewski et al., 1993)
Mn_3O_4	I 41/a m d S	−700.2	−693.7 (Kubaschewski et al., 1993)
Mn_2O_3	P b c a	−654.4	−638.7 (Kubaschewski et al., 1993)
Mn_5O_8	C 1 2/m 1	−619.6	
MnO_2	I 4/m	−523	−520.9 (Kubaschewski et al., 1993)
Mn_2O_7	P 1 21/c 1	−212.7	
Na_2O	F m −3 m	−864	−830.2 (Kubaschewski et al., 1993)
NaO	P -6 2 m	−567	−513 (Kubaschewski et al., 1993)
NaO_2	P n n m	−374.4	−260.7 (Kubaschewski et al., 1993)
NaO_3	I m 2 m	−291	
NiO	R −3m R	−479.4	−479.4 (Kubaschewski et al., 1993)
NiO_2	C 1 2/m 1	−220.7	
Pd_2O	P n −3 m S	−222.6	
PdO	P 42/m m c	−304.3	−231 (Kubaschewski et al., 1993)
PtO	P 42/m m c	−225	
Pt_3O_4	P m −3 n	−284.6	
PtO_2	P n n m	−268.5	
Rb_6O	P 63/m	−693.7	
Rb_9O_2	P 1 21/m 1	−692.4	
Rb_2O	F m −3 m	−646.7	−677.8 (Kubaschewski et al., 1993)
RbO	I m m m	−510.9	−472 (Dean, 1999)
Rb_2O_3	I −4 3 d	−426.8	
RbO_3	P 1 21/c 1	−296.7	
Rh_2O_3	P b n a	−348.9	−237.1 (Kubaschewski et al., 1993)
RhO_2	P 42/m n m	−354.3	
Sc_2O_3	I 21 3	−1278.5	−1272.2 (Kubaschewski et al., 1993)
SrO	F m −3 m	−1190.4	−1184 (Kubaschewski et al., 1993)
SrO_2	I 4/m m m	−680.7	−633.5 (Kubaschewski et al., 1993)
Ti_6O	P 3 1 c	−1223.8	
Ti_3O	P −3 1 c	−1205.2	
Ti_2O	P −3m 1	−1173	
TiO	A 1 1 2/m	−1096.7	−1085.4 (Kubaschewski et al., 1993)
Ti_4O_5	I 4/m	−1065.4	
Ti_2O_3	R −3 c H	−1048	−1013.9 (Kubaschewski et al., 1993)
Ti_3O_5	C 1 2/m 1	−1023.9	−983.6 (Kubaschewski et al., 1993)
Ti_4O_7	P −1	−1012.8	−972.7 (National Institute of Standards Technology, 2009)
Ti_5O_9	P −1	−1006.2	
Ti_6O_{11}	C 1 2/m 1	−1002.1	
Ti_7O_{13}	P −1	−998.4	
Ti_8O_{15}	I −1	−996	
Ti_9O_{17}	P −1	−993.7	
TiO_2	C 1 2/m 1	−985.4	−944 (Kubaschewski et al., 1993)
Tl_2O	R −3m H	−495.5	−334.8 (Kubaschewski et al., 1993)
Tl_4O_3	P 1 21/m 1	−431.1	
Tl_2O_3	I 21 3	−342.2	−260.3 (Kubaschewski et al., 1993)
Y_2O_3	I a −3	−1280.1	−1270 (Kubaschewski et al., 1993)
Zr_3O	R −3 c H	−1234.8	
Zr_2O	P n −3m S	−1044.1	
ZrO	F m −3 m	−1026.1	
ZrO_2	P 1 21/c 1	−1116.5	−1100.8 (Kubaschewski et al., 1993)

References

ASM International, 2009. ASM Alloy Phase Diagrams Center; 〈http://www.asminternational.org/AsmEnterprise/APD〉.

Baltrus, J.P., et al., 2008. Surface characterization of Pd/Al_2O_3 sorbents for mercury capture from fuel gas. Main Group Chemistry 7 (3), 217–225.

Bergerhoff, G., et al., 1983. The inorganic crystal-structure data-base. Journal of Chemical Information and Computer Sciences 23 (2), 66–69.

Binnewies, M.M.E., 1999. Thermochemical Data of Elements and Compounds. Weinheim, New York.

Blochl, P.E., 1994. Projector Augmented-Wave Method. Physical Review B 50 (24), 17953–17979.

Curtarolo, S., 2003. Coarse-graining and data mining approaches to the prediction of structures and their dynamics. Dissertation/Thesis, Massachusetts Institute of Technology.

de Boer, F.R., et al., 1988. Cohesion in Metals: Transition Metal Alloys. North Holland.

Dean, J.A., 1999. Lange's Handbook of Chemistry, 15th ed. McGraw-Hill.

Dudarev, S.L., et al., 1998. Electron-energy-loss spectra and the structural stability of nickel oxide: an LSDA+U study. Physical Review B 57 (3), 1505–1509.

Electric Power Research Institute, 1998. Materials Guidelines for Gasification Plants. Palo Alto, CA.

Ellingham, H.J.T., 1944. Reducibility of oxides and sulphides in metallurgical processes. Journal of the Society of Chemical Industry 63.

Environmental Protection Agency, 2009. 〈http://www.epa.gov/mercury/regs.htm〉.

Environmental Protection Agency, 2005. Clean Air Mercury Rule.

Environmental Protection Agency, 2006. State Clean Energy–Environment Technical Forum: Integrated Gasification Combined Cycle (IGCC) Background and Technical Issues.

Fermi, E., 1956. Thermodynamics. Dover Publications.

Fischer, C.C., et al., 2006. Predicting crystal structure by merging data mining with quantum mechanics. Nature Materials 5 (8), 641–646.

FIZ Karlsruhe, 2009. ICSD Inorganic Crystal Structure Database; 〈http://icsdweb.fiz-karlsruhe.de/index.php〉.

Fujii, S., Ishida, S., Asano, S., 1991. Magnetic states in bcc manganese. Journal of the Physical Society of Japan 60 (4), 1193.

Gaston, N., et al., 2006. Lattice structure of mercury: influence of electronic correlation. Physical Review B (Condensed Matter and Materials Physics) 74 (9), 094102–094109.

Granite, E.J., Hargis, R.A., Pennline, H.W., 1998. Sorbents for mercury removal from flue gas.

Granite, E.J., Pennline, H.W., Hargis, R.A., 2000. Novel sorbents for mercury removal from flue gas. Industrial and Engineering Chemistry Research 39 (4), 1020–1029.

Granite, E.J., et al., 2006. Sorbents for mercury capture from fuel gas with application to gasification systems. Industrial and Engineering Chemistry Research 45 (13), 4844–4848.

Hafner, J., Wolverton, C., Ceder, G., 2006. Toward computational materials design: the impact of density functional theory on materials research. MRS Bulletin 31 (9), 659–665.

Hultgren, R.D., Pramod, D., Hawkins, Donald T., Gleiser, Molly, Kelley, Kenneth K., 1973. Selected values of the thermodynamic properties of binary alloys. American Society for Metals.

International Energy Agency, 2008. World Energy Outlook 2008, 569th ed. Organization for Economic Co-operation and Development.

Kresse, G., Furthmuller, J., & January. VASP the GUIDE, vol. 2007.

Kresse, G., Furthmuller, J., 1996. Efficiency of ab-initio total energy calculations for metals and semiconductors using a plane-wave basis set. Computational Materials Science 6, 15.

Kresse, G., Joubert, D., 1999. From ultrasoft pseudopotentials to the projector augmented-wave method. Physical Review B 59 (3), 1758–1775.

Kubaschewski, O., Alcock, C.B., Spencer, P.J., 1993. Materials Thermochemistry. Pergamom Press.

Lee, J-Y., Ju, Y., Lee, S-S., Keener, T.C., Varma, R.S., 2008. Novel mercury oxidant and sorbent for mercury emissions control from coal-fired power plants. Water Air and Soil Pollution: Focus 8, 333–341.

Mitchell, B.S., 2004. An Introduction to Materials Engineering and Science for Chemical and Materials Engineers (Illustrated ed.). Wiley – IEEE.

National Institute of Standards and Technology, 2009. NIST Chemistry Webbook, NIST Standard Reference Database no. 69; 〈http://webbook.nist.gov〉.

Nexant Inc., 2006. Environmental footprints and costs of coal-based integrated gasification combined cycle and pulverized coal technologies. Environmental Protection Agency.

O'Dowd, W.J., et al., 2004. Recent advances in mercury removal technology at the National Energy Technology Laboratory. Air Quality III: Mercury, Trace Elements and Particulate Matter 85 (6-7), 533–548.

Parsons Infrastructure & Technology Group Inc, 2002. The Cost of Mercury Removal in an IGCC Plant. US DOE National Energy Technology Laboratory.

Pavlish, J.H., et al., 2003. Status review of mercury control options for coal-fired power plants. Fuel Processing Technology 82 (2–3), 89–165.

Perdew, J.P., Burke, K., Ernzerhof, M., 1996. Generalized gradient approximation made simple. Physical Review Letters 77 (8), 3865–3868.

Portzer, J.W., et al., 2004. Development of novel sorbents for mercury control at elevated temperatures in coal-derived syngas: results of initial screening of candidate materials. Fuel Processing Technology 85 (6–7), 621–630.

Poulston, S., et al., 2007. Metal sorbents for high temperature mercury capture from fuel gas. In: The 6th European Conference on Coal Research and its Applications, 86(14), pp. 2201–2203.

Powell, C.A., Morreale, B.D., 2008. Materials challenges in advanced coal conversion technologies. MRS Bulletin 33 (4), 309–315.

Presto, A.A., Granite, E.J., 2008. Noble metal catalysts for mercury oxidation in utility flue gas. Platinum Metals Review 52, 144.

Schlather, J., Turk, B., 2007. Comparison of a new warm-gas desulfurization process versus traditional scrubbers for a commercial IGCC Power Plant.

Schlather, J., Turk, B., 2007. Comparison of a new warm-gas desulfurization process versus traditional scrubbers for a commercial IGCC Power Plant. In: Proceedings of Gasification Technologies Conference, San Francisco, 2007. 〈http://www.gasification.org/Docs/Conferences/2007/55SCHL.pdf〉.

Soverna, S., et al., 2005. Thermochromatographic studies of mercury and radon on transition metal surfaces. Radiochimica Acta 93 (1), 1–8.

Steckel, J.A., 2008. Density functional theory study of mercury adsorption on metal surfaces. Physical Review B 77 (11), 115412.

Valkov, V.I., Golovchan, A.V., 2005. Interplay between the spin state of manganese and the stability of the crystal structure of MnAs and MnP compounds. Low Temperature Physics 31 (6), 528–533.

Velasco, S., et al., 2006. Prediction of the enthalpy of vaporization of metals and metalloids. Fluid Phase Equilibria 244 (1), 11–15.

Wang, L., Maxisch, T., Ceder, G., 2006. Oxidation energies of transition metal oxides within the GGA+U framework. Physical Review B 73 (19), 195107.